Suppression of phase ambiguity in digital holography by using partial coherence or specimen rotation

Zeev Zalevsky,[1,*] Ofer Margalit,[1] Emanuel Vexberg,[1] Roy Pearl,[1] and Javier Garcia[2]

[1]School of Engineering, Bar-Ilan University, Ramat-Gan 52900, Israel

[2]Departamento de Óptica, Universitat de València, c/Dr. Moliner, 50, 46100 Burjassot, Spain

*Corresponding author: zalevsz@eng.biu.ac.il

Received 27 September 2007; revised 8 March 2008; accepted 12 March 2008; posted 18 March 2008 (Doc. ID 87928); published 22 April 2008

In this paper we present two approaches for extracting the surface profile as well as obtaining 3D imaging of near field objects by usage of partial coherence and digital holography. In the first approach a light source with given temporal partial coherence is used to illuminate a near field object. The reflected light is interfered with the reference source. By computing the local contrast of the generated fringes one may estimate the 3D topography and the profile of the object. This approach extracts the 3D information from a single image, and its accuracy does not depend on triangulation angle like in fringe projection methods. The second approach is tomography based. There we illuminate the object from several slightly different angles, and for each we compute the wrapped phase using digital holography techniques. Combining the wrapped phase estimation from several points of projection allows calculating the unwrapped phase and therefore the true profile of even a phase-only object. Increasing the number of points of view decreases the relative error of the estimated profile. © 2008 Optical Society of America

OCIS codes: 090.1995, 150.6910, 030.1640, 110.5086.

1. Introduction

There is a very large variety of techniques for 3D and range estimation. Therefore, we will mention only some of them. One common approach includes projection of a grating and computing the gradients obtained in the image [1–5]. The main disadvantage of this type of estimation is that the gradients are obtained only in locations with height changes that are usually very space limited and shadowed. Since the height estimation in this approach is cumulative, a miss of a certain gradient (height change) accumulates an error. In addition the technique will obtain the height change only in the direction perpendicular to the projected grating. If the height change coincides with the grating direction no gradient will be obtained.

Other 3D techniques involve projection of a line on the object and scanning the object with that line. The height might be obtained based on the curvature of the projected line [6–11]. The main problem with those approaches is in the fact that the object must be static during the scanning process, otherwise the height estimation is blurred. Such approaches will not work for motion estimation.

Another technique is high speed scanning based on active laser triangulation and a variety of fast to even real-time scanners [12]. A completely different approach is based upon stereometric structured light technique where active projection of patterns is viewed from various angles by the camera [13,14]. The accuracy of all previously mentioned techniques depends on the angle between the object and the projector and the camera or, as in triangulation [15–17], on the angle that the object creates with the two cameras.

Some other approaches are based upon diffractive optical elements that project a pattern that varies along the axial direction of light's propagation and that way the type of pattern seen by the camera provides the designation of the distance [18]. However,

0003-6935/08/19D154-10$15.00/0

in this type of approach the axial resolution of range estimation as well as the transversal resolution are very limited.

Holography allows the extraction of the phase of the object, although the recording is done in intensity [19–23]. In analog holography the recording of an intensity pattern that is a result of interference is done on a photo film, while a reference beam is projected side by side with the light reflected from the object. The reconstruction is done by illuminating the film with the same reference beam. In digital holography [24] the interference pattern generated from the object and the reference wave is recorded onto an image sensor, and reconstruction is done with a computer by numerical propagation methods (e.g., convolution [25,26], angular spectrum [27], and Fresnel–Kirchhoff [28,29]). The worse resolution of digital imaging media as compared with analog holographic media limits the maximum angle between interfering beams to a few degrees.

The use of an in-line setup permits the measurement of the object complex amplitude distribution by using phase shifting interferometry [30,31]. Similarly, Iemmi *et al.* [32] applied a point diffraction interferometer to digital holography using phase shifting steps controlled by means of a liquid crystal device (LCD). That way they could obtain both amplitude and phase distributions and visualization of a 3D object by simple propagation of the calculated distributions using computer tools. One of the most useful applications of digital holography is microscopy. Digital in-line microscopy with numerical reconstruction [33,34] provides a powerful technique for lensless imaging when a low-density object is imaged. Note however that digital holographic microscopy is also done in off-axis geometry, for example as presented in [35–38].

Another interesting approach for 3D is based upon using the coherence of a light source. If the coherence length is short, only surface variations that are smaller than this length will generate interference fringes [39,40]. By shifting the sample each time, the fringes will appear in different transversal locations and the 3D topography of the sample can be mapped. For example, in optical coherence tomography [41,42], the coherence length of the light source is used in order to interfere only with light reflected from a very certain layer inside the biomedical sample. A similar concept is used in digital holography, where 3D topography of the sample can be mapped without transversal scanning [43,44]. In addition, various papers were also published about tomography in digital holography where rotation of the specimen or modification of the illuminated wave was used to extract the profile [45–47].

In this paper we present two approaches that are related to digital holography in order to estimate the 3D profile of reflective as well as transmissive objects. The first approach is based upon illuminating a reflective object with light source of given coherence length. The coherence length may be relatively long. However, the contrast of the fringes within this length will vary. We map our source by measuring the contrast of the interference fringes versus axial position. This will now be our lookup table for the 3D estimation. Now, after placing our reflective object into the system we capture a single image (we do not shift the object and scan as in [48]) and compute the locale contrasts of the fringes. By comparing this contrast with the lookup table we extract the 3D information. This approach extracts the 3D information from a single image, and its accuracy does not depend on the triangulation angle.

The second approach deals with a technique allowing extraction of profile of transmissive objects especially in microscopy and mainly with biomedical and cell research, where in many cases the sample is transparent (phase-only objects). The approach resembles the concept of tomography [49]. We use digital holography in order to extract the phase profile obtained from an object while we slightly vary the angle of the specimen. The profile of the sample is extracted from at least two angles despite the fact that the profile variations generate phase changes of more than 2π. Actually the usage of at least two angles is required in order to solve the phase wrapping ambiguity existing in all the other approaches such as phase shifting [30].

If the sample is uniform in its profile and there is variation only in the refraction index, this approach can be used as well in order to estimate the refraction index of the transparent sample (various approaches exist for determination of the refractive index in digital holography such as in [38,50–53]). By using more than two angles, the precision for the profile estimation (or for the refraction index) is increased. Applying the proposed approach in microscopy for research of cells offers several advantages such as imaging of phase-only objects without the need to translate the phase information into an amplitude information, extraction of the true profile without phase wrapping ambiguities, and possibility for estimating the refraction index.

In Section 2 we present the theory and explain the operation principle of each one of the two approaches. In Section 3 we present some preliminary experimental results. The paper is concluded in Section 4.

2. Operation principle

A. Partial coherence for 3D

The first approach that is presented in this paper deals with extraction of 3D information based upon the partial coherence of the light source. Assuming two interfering beams, the resulting field distribution equals

$$E_{tot}(x,t) = A_1 \exp(i\phi_1(t)) \exp\left(\frac{2\pi i \times \sin\theta}{\lambda} x\right) + A_2 \exp(i\phi_2(t)) \exp\left(\frac{-2\pi i \times \sin\theta}{\lambda} x\right), \quad (1)$$

where A_i, φ_i are the amplitude and the phase of each beam, respectively; λ is the wavelength; and θ is the difference between their angles of arrival to the detection plane. The intensity in this case equals

$$I_{tot}(x) = \langle E_{tot}(x,t) E^*_{tot}(x,t) \rangle = A_1^2 + A_2^2 + 2A_1A_2 \langle \cos(\phi_1(t) - \phi_2(t)) \rangle \cdot \cos\left(\frac{4\pi \sin\theta}{\lambda} x\right), \quad (2)$$

where $< \ldots >$ designates time averaging operation. For two coherent sources: $\langle \cos(\phi_1(t) - \phi_2(t)) \rangle = \cos(\phi_1 - \phi_2)$, and for incoherent sources $\langle \cos(\phi_1(t) - \phi_2(t)) \rangle = 0$. Therefore it is clear that the amount of coherence determines the contrast of the generated interference fringes.

Given a certain laser, its coherence length inversely depends on its spectral bandwidth (its colors' content). What we propose in this technique is an approach for mapping the 3D information of reflective objects. We assume that only a single interference image is captured. Since we are talking about reflective objects (and not diffusive) no imaging lens is needed for the setup in order to relate the contrast of the interference fringes and the resulting 3D profile with the spatial coordinates of the object.

Basically we use Michelson's interferometer configuration, where there is a mirror in the reference path and an object in the second optical path. Since $\lambda/(2\sin\theta)$ is the spatial period of the fringes we will use a relatively large angle difference θ (of, say, a few degrees, e.g., 1°) such that the interference fringes are obtained with high spatial frequency and therefore high spatial lateral resolution for the 3D mapping (for instance with an angle of 1° we may have spatial lateral resolution of 15 μm for a wavelength of 500 nm),

We start by calibrating our system and instead of an object we place a mirror (therefore the setup is a Michelson interferometer with two mirrors both in the reference plane and in the object path). We scan with the mirror and map the change of the local spatial contrast of the interference fringes versus the axial position of the reference mirror. This result will be used as our lookup table for later on to translate the contrast of the image to real 3D information of the reflective object. The smaller the axial range we wish to map, the shorter should be the coherence length of our light source.

After computing the lookup table, we place the object back into the interferometer setup (we take out the mirror that before was temporally placed in its position) and capture a single image. We compute the local contrast of the fringes for every transversal position in the captured image. By comparing the result with our lookup table the profile of the object may be estimated. Note that by tuning the spectral width of our light source we vary its coherence length, and therefore we can control or adjust the axial range that is usable for the 3D mapping.

The proposed approach is good for extracting the 3D information or the profile of reflective objects, while its main application can be in the field of microscopy or in the microelectronic industry (inspection of various wafers) since the shorter the coherence length, the better the axial resolution. The main advantage of this approach in comparison with other approaches is that it does not use triangulation, and therefore its precision is not dependent on the angle between the object and the two cameras [15–17] or the camera and the projection module [6]. Another advantage is that the 3D information is extracted from a single image, while no axial scanning is required [48], and therefore this method may be used for real time mapping of live specimens.

Note that since lasers usually have several spectral lines (due to their Fabry–Perot interferometer), the coherence length is a periodic function, while its period inversely depends on the total spectral width of the source (the spectral separation between the lines multiplied by the number of lines) and the overall number of periods inversely depends on the width of each spectral line (actually it will be the ratio between the total spectral width and the width of each spectral line). In our experiments for the demonstration of this approach we used Nd:YAG laser with axial periodicity for the coherence function of close to 2 mm (overall spectral width of about 150 GHz). The coherence length should be application dependent. For instance, for application of chip inspection (in microelectronics) or for microscopy, the coherence length should be in the range of about 0.1 mm For application of pattern recognition, computer vision, and gaming, the range should be a few tens of cm or even more.

An important comment is related to the relation between the lateral field of view and the axial resolution obtained by this approach. Across the field of view the fringes do not have uniform contrast since rays coming to the external regions of the field of view travel longer optical paths in comparison with the rays coming to the center of the field. The difference of the contrast along the field of view can be mapped as part of the calibration process in which the lookup table is prepared. However, the field of view must be limited such that for a given coherence length and thus for a given axial resolution the fringes at the borders of the field of view will still have detectable contrast. Mathematically, given a sensor having b sampling bits, i.e., 2^b gray levels of dynamic range, and angle of θ between the two interfering optical paths, and a sensor with a lateral dimension of L, the best possible axial resolution δz that may be obtained will be

$$\delta z \approx \frac{L \times \sin\theta}{2^b}, \quad (3)$$

which means that the contrast of the fringes at the edges of the image should not be below the minimal level of quantization.

Another important note is related to the number of sampling pixels. In every period of the interference fringes one needs more than 2 sampling pixels (at least twice as much as required by Nyquist's sampling theorem) in order to estimate the contrast. The double number of pixels is needed to have sufficiently accurate estimation. Therefore if the angle between the two interfering paths is 1° and thus the period of the fringes is $15\,\mu$m for a wavelength of 500 nm, then the size of the pixels should not be larger than about $4\,\mu$m in order to have sufficient samples for the contrast estimation. Thus, since $4\,\mu$m is about the smallest available pixel size, the value of about $15\,\mu$m is the maximal lateral resolution for the 3D mapping.

Since the 3D mapping in this approach is based upon local contrast estimation, the reflectivity of the objects can affect this estimation, and it must be addressed in the calibration stage as well as in the profile estimation procedure. In the next section, in Eqs. (7) and (8) we demonstrate that in proper computing procedure this effect is not too significant. We show that even in the extreme case of a silicon wafer having reflectivity of only 30% for intensity and a mirror in the reference path having reflectivity of 100%, the effect over the contrast estimation is only 15%. Therefore, if the inspected object comprises several materials, each having a different refraction index and therefore different reflectivity, the maximal error will be smaller than 15% [e.g., see experimental results of Fig. 5(a)]. In the real case the variation in the reflectivity will not be 70% (100% in comparison with 30%) but rather smaller than that, which will affect the estimation by only a few percent. By proper normalization the generated error may be reduced (e.g., by estimating the contrast in plurality of neighbor sampling points and averaging the results).

The proposed technique does not include an imaging lens, and therefore the lateral resolution for the 3D mapping is affected not only by the coherence of the source or the capability to estimate local contrast but also by the diffraction, which blurs spatial features especially near steep borders. The blurring spot or the spatial resolution δx_z that is forced by the diffraction after free space propagation of a distance of Z can be estimated by the following relation:

$$\delta x_z = \sqrt{\delta x^2 + (\lambda Z/(2\pi \cdot \delta x))^2}, \tag{4}$$

where δx is the standard deviation of the smallest spatial feature in the original object (we assume a Gaussian distribution), λ is the optical wavelength, and Z is the free space propagation distance. In order not to lose resolution one needs

$$Z \leq \frac{2\pi \cdot \delta x^2}{\lambda}, \tag{5}$$

assuming again spatial resolution of $\delta x = 15\,\mu$m and wavelength of 500 nm, the length of the free space path should not be larger than approximately $Z = 3$ mm. Basically, even such short propagation distances may be feasible in real configurations (with small beam splitters that can be integrated on top of the detection array). However, in the proposed setup the dimensions of the beam splitter prevent us of going to Z being below 1 cm. Therefore, the spatial resolution will be reduced to $\delta x = 30\,\mu$m.

B. Phase unwrapped profiling

Phase-shifting and holography-based approaches are used for extraction of 3D information. The main problem of those approaches is the phase wrapping, i.e., the mapping range should not be larger than one wavelength otherwise there is an ambiguity [30]. Therefore such approaches are not suitable for profile estimation having a large range of topographic variations. Here we suggest using a tomography-based approach in order to solve the phase wrapping ambiguity.

The idea is to project a transmissive object whose profile we wish to extract, from several angles. Then, by digital holography to recover the phase of every exposure. The phase recovery by digital holography includes performing a Fourier transform over the fringe pattern and then taking out the information around the first diffraction order, putting it around the center of the axes, and performing the inverse Fourier transform. The obtained result is back free space propagated (using the Fresnel transform) a free space distance that exists between the specimen and the recording array. The phase after the back free space propagation is extracted, and it is the result for the desired phase that is related to the profile of the inspected object.

The angular change between the sequential exposures is very small since we require that the transversal shift caused due to the change in angle will be less than one pixel in the camera. This requirement is important in order to be able to compare the images one on top of the other without additional image registration processing requirements (which can be applied in case that this condition is not fulfilled). This requirement is schematically demonstrated in Fig. 1. From at least two angles the ambiguity of the phase can be solved. Increasing the number of the angles increases the accuracy of the profile estimation.

The main advantage of this approach is that it can be used for completely transparent objects (phase objects) to estimate their profile. On the other hand if

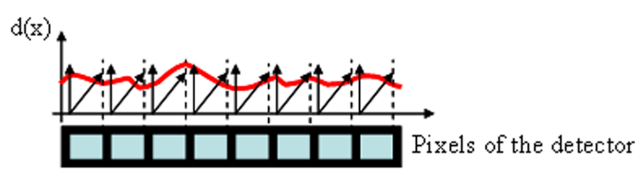

Fig. 1. (Color online) Schematic illustration of the projections through the sample. The angular difference should not be too large such that the two reconstructed patterns will not be shifted more than a pixel.

the profile is known, this technique can be used in order to estimate the refraction index of the phase specimen [45–47]. The main application is in microscopy for biomedical applications where this procedure can assist in imaging the phase-only samples without the need to translate the phase information into amplitude information. This approach may also be used in the microelectronics industry especially for wafer inspection.

The optical configuration is basically a Mach–Zehnder interferometer where the sample is placed on a rotating stage and its angle of position can be accurately tuned. Assuming that a sample is illuminated at two different angles θ_1 and θ_2, then two phase readouts can be extracted (one per each image) after proper processing (as done in digital holography). We denote by $a(x)$ and $b(x)$ the phase extracted in the first and the second projection, respectively:

$$\left\{\frac{2\pi n d(x)}{\lambda \cos\theta_1}\right\}\mathrm{mod}\{2\pi\} = a\,(x),$$
$$\left\{\frac{2\pi n d(x)}{\lambda \cos\theta_2}\right\}\mathrm{mod}\{2\pi\} = b(x), \tag{6}$$

where λ is the wavelength, n is the refraction index of the sample, and $d(x)$ is the true (unwrapped) profile that we wish to extract. mod is the mathematical operation of modulo.

Plotting the theoretical a and b values for width d varying from $0.5\,\mu$m up to $20\,\mu$m in steps of 10 nm yields the result presented in Fig. 2. One may see that indeed the mapping is one to one and comparing the measured a and b values with the existing lookup table can lead to the estimation of d.

It is clear that increasing the number of angles reduces the estimation error. Assuming that one uses M angles, then the number of possible combinations of a pair of angles will be equal to $M(M-1)$, and

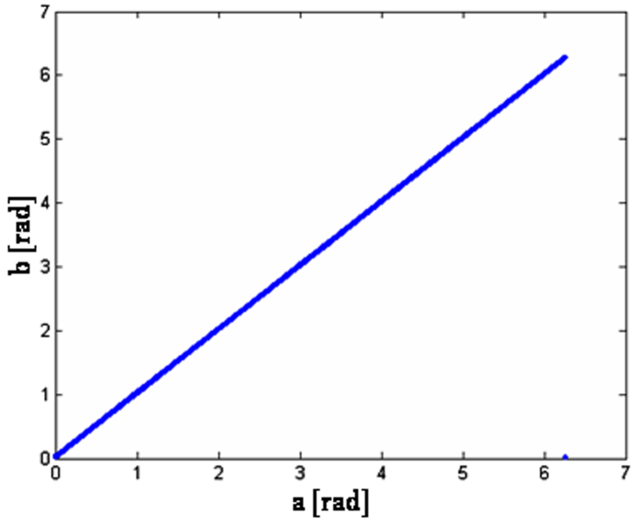

Fig. 2. (Color online) One to one mapping between various heights of the profile $d(x)$ and the readout phases $a(x)$ and $b(x)$.

therefore since each one of those combinations will produce an uncorrelated estimation for the profile d, the overall error will be reduced by a factor of $\sqrt{M(M-1)-1}$.

3. Experimental investigation

A. Partial coherence for 3D

An experimental setup that is based upon Michelson interferometer was constructed in the lab (see in Fig. 3 both the schematic sketch of the setup and its real image). As opposed to the setup in [48], no imaging lens is needed since we deal with reflective rather than diffusive objects. First, we have constructed the lookup table by placing a mirror instead of the object and axially shifting (i.e., scanning with) the mirror of the reference beam while measuring the contrast for all of its axial positions. We used

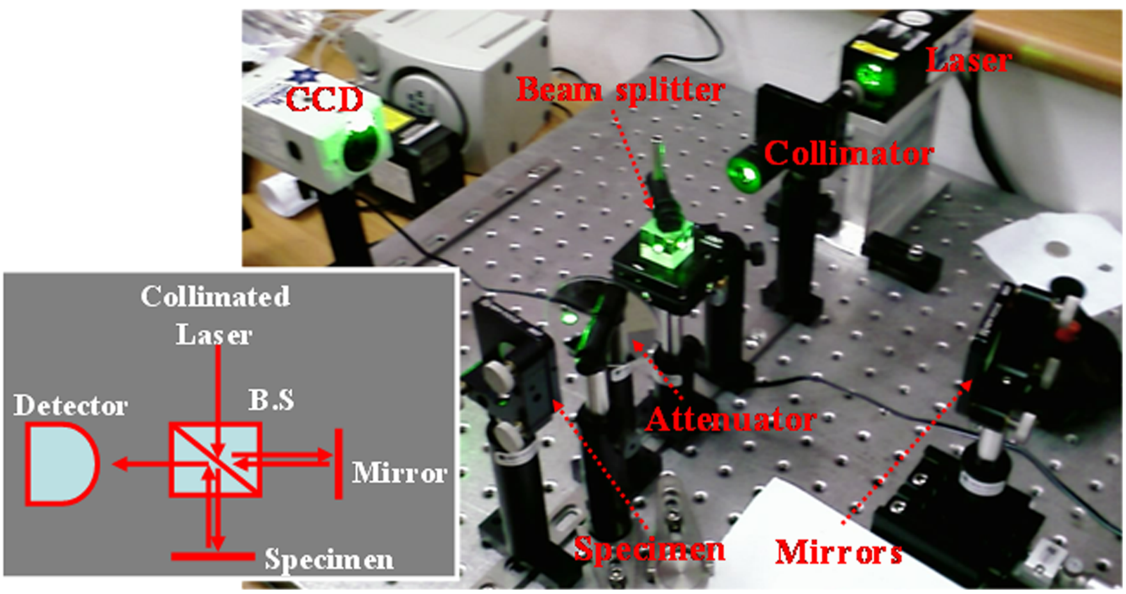

Fig. 3. (Color online) Experimental setup for the partial coherence experiment. B.S, beam splitter.

an Nd:YAG laser at a wavelength of 512 nm. The contrast chart versus the axial shift appears in Figs. 4(a) and 4(b). Actually we did this measurement twice for two different alignments of the setup. Obviously the contrast and the lookup table depend on the specific alignment of the optical setup.

In the next step we placed a reflective object containing several silicon wafers (taken from the microelectronics industry). We performed two experiments; in the first the two wafers were positioned side by side on top of a mirror. In the second experiment we used three wafers, two placed on top of the third one.

As previously mentioned a very interesting property of the proposed configuration is that it almost does not depend on the exact reflectivity of the surface of the object that we map. What we mean is that the spatial contrast variations mainly depend on the topography rather than the reflectivity profile of the object. This is a very important property since otherwise the method would not have been that applicable. Let us now mathematically estimate the sensitivity to the reflectivity of the inspected object. The contrast C is defined as

$$C = \frac{I_{\max} - I_{\min}}{I_{\max} + I_{\min}} = \frac{2|r_1 r_2|}{|r_1|^2 + |r_2|^2}, \qquad (7)$$

where $I_{\max}$ and $I_{\min}$ are the maximal and the minimal intensities, respectively, of the interference fringe. r_1 and r_2 are the fields' reflectivity for the two optical paths of the interferometer. This is of course in the case of perfect alignment and ideal conditions. In our experiments we used silicon wafers, while the lookup table was obtained with mirrors. The reflectivity of silicon can be computed using Fresnel coefficients. At normal angles

$$|r| = \left|\frac{n_1 - n_2}{n_1 + n_2}\right|. \qquad (8)$$

In the case of silicon surrounded by air we have approximately $n_1 = 3.5$ and $n_2 = 1$, and therefore $|r| = 0.556$. In the case of the mirror, the reflectivity coefficient $|r|$ is close to 1. If we place those numbers in Eq. (7) we see that instead of having maximal contrast of 1 we will have a contrast of 0.85. Therefore, in the extreme case of a perfect mirror and a silicon wafer which is far from being a mirror, the variation due to the change in the object's reflectivity is only by 15%. Obviously in the practical case this difference is much smaller since the mirror's reflectivity is not exactly 1 and the alignment is not perfect. Also when we know the type of substrate (e.g., silicon) we can perform a normalization of contrasts according to the ratio from Eq. (7).

Note that in the visible range the silicon will have not only a real but also an imaginary part (attenuation) for the refractive index. However, the imaginary part of the refractive index is about 200 times smaller than the real part and therefore was neglected in our computation.

Following this line we performed two experiments with silicon wafers. The thickness of each wafer was 765 μm with standard variation for the thickness of 10 μm. In both experiments the objects were placed in the setup (each in turn) and the interference pattern was captured. The local contrast of the fringes was computed, and it was compared with the results from the lookup table of Figs. 4(a) and 4(b). Since the orientation or the tilting angles of the fringes are unknown and they are varied along the captured image, the estimation of the local contrast in an automatic manner was not trivial. Our solution for this problem was to use the Radon transform for the computation of the local contrasts (the Radon transform produces a high value if the direction of its projections is parallel to the direction of the interference fringes). Therefore the Radon transform assisted us in automatic allocation of the tilting direction of the fringes such that correct computing of contrast was feasible. An example of fringes and their corresponding Radon

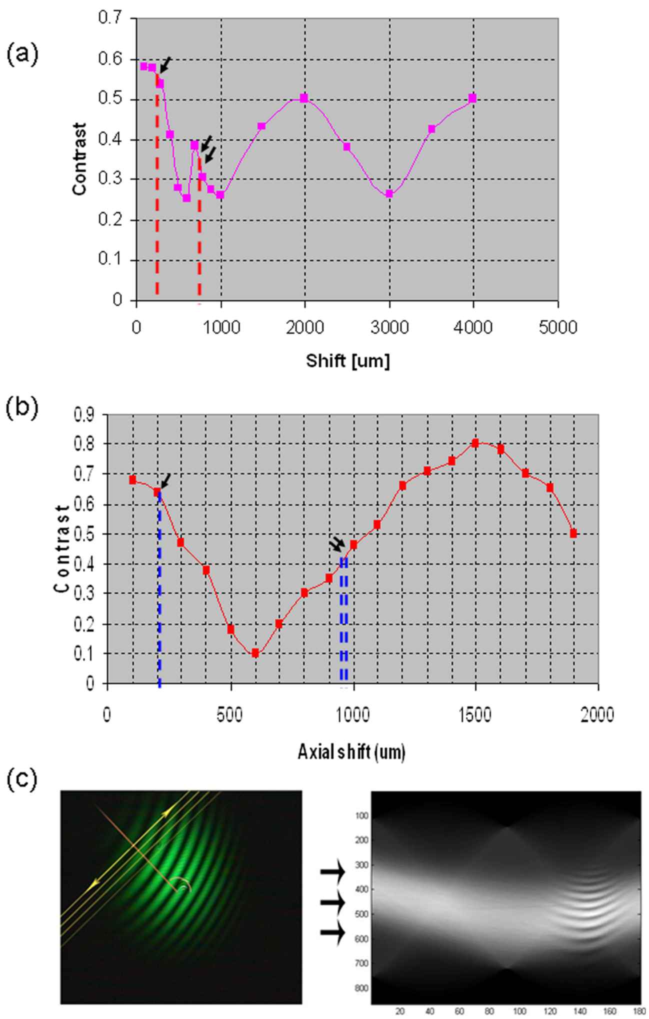

Fig. 4. (Color online) Experimental mapping of the contrast chart versus the axial shift of one of the mirrors. (a) and (b) are for two different alignments. (c) Fringes and their corresponding Radon transform.

transform (to be used for the estimation of the contrast) is presented in Fig. 4(c). At the angles corresponding to the tilting of the fringes, at the Radon transform one will get a periodic pattern with high values of gray levels. At that angle the contrast should be computed, and this is the tilting angle of the fringes. After computing an image of local contrasts, a topography image for the specimen can be extracted.

The experimental results, including the image of the object and the interference pattern of the fringes as well as the numerical extraction of the local contrasts, appear in Fig. 5. The image in Fig. 5(a) corresponds to the alignment, and the lookup table of Fig. 4(a), and the image of Fig. 5(b) corresponds to the alignment of 4(b). After the measurements of the local contrast we saw in both cases that indeed:

- In Fig. 5(a) the difference in thickness between the two small silicon wafers and the mirror is around 765 μm (as anticipated), while the difference between the two wafers (upper left and upper right) is approximately of the order of magnitude of 20–30 μm. This is obtained by comparing the reference chart of Fig. 4(a) with the measurements of the contrast in Fig. 5(a). The relevant values were marked on the chart in Fig. 4(a).
- In Fig. 5(b) the difference in thickness between the wafer on the left side and the two wafers on the right side is approximately 765 μm (as anticipated), while the difference in the thickness of the two wafers on the right side (right/up and right/ down) is about 10–15 μm. This is obtained by comparing the reference chart of Fig. 4(b) with the measurements of the contrast in Fig. 5(b). The relevant values were marked on the chart in Fig. 4(b).

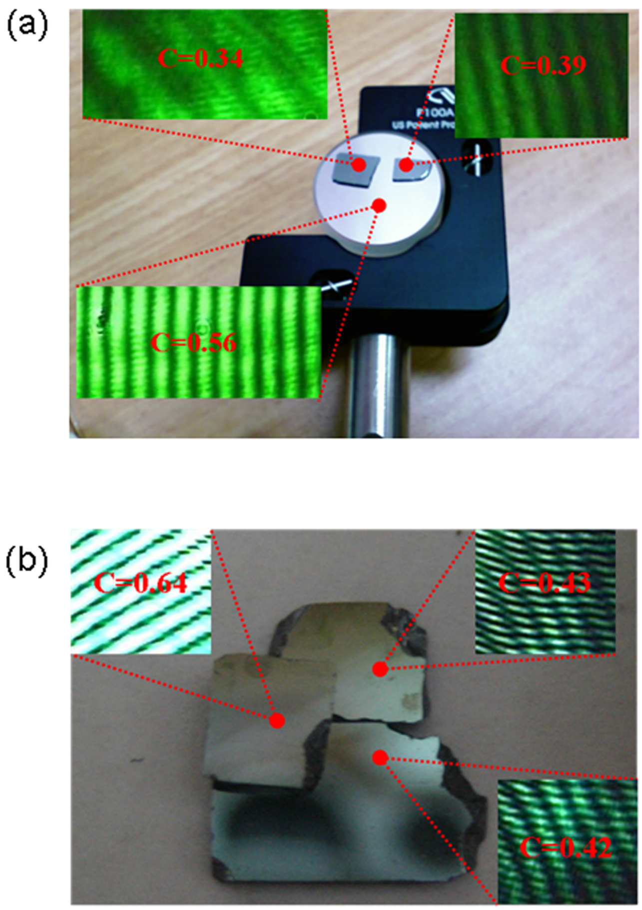

Fig. 5. (Color online) Image of the object used for the partial coherence experiment and the obtained interference pattern with the extracted local contrasts. (a) Two silicon wafers positioned on a mirror. (b). Two silicon wafers positioned on top of a third silicon wafer.

Note that since the lookup charts of Figs. 4(a) and 4(b) are periodic, there are several positions that have had the contrast values (of Fig. 5(a) and 5(b)) measured, each resulting in a different possible result for the height estimation. In general, in the proposed approach we do not intend to go beyond half a period of the reference lookup charts, i.e., beyond half the period of the axial coherence length, and that way we intend to avoid interpretation ambiguity. It is even recommended to have the working zone much smaller than that in order to stay in the linear region of the lookup (i.e., calibration) chart in order to have a linear relation between the changes in contrast and their corresponding height/topography interpretation. The object that we tested in our preliminary experiment did not have perfect fit to the coherence length of our laser, and therefore some ambiguity in interpretation was generated. By looking in the *a priori* known range we could estimate the precise value of the profile. Obviously in a real application proper fitting should be made between the coherence length of the source and the range of profiles that we aim to inspect in our specimen. In addition, generally speaking the lookup tables have a discrete set of values. Therefore, if the measured contrast falls in between two values of the table an interpolation procedure is applied in order to have the precise profile estimation. Also note that the experimental setup of Fig. 3 is used only for reflective objects such as those that we took from the silicon industry. The 3D information was extracted from a single image, and therefore it is useful for real time inspection applications.

B. Phase unwrapped profiling

The experiment included construction of Mach–Zehnder-based interferometer, while the sample to be inspected was placed on top of a high precision rotation stage. The image of the setup appears along with its schematic sketch in Fig. 6. We used a He–Ne laser with a long coherence length (more than a few tens of cm). The inspected object was a small rectangle generated in photolithography process on top of a glass substrate. The refraction index of the glass substrate was 1.5, while that of the photoresist was 1.6 (after developing). The photoresist used was SU-8. For comparison, the profile of the rectangle was mapped using an Alpha-Step profile meter and ap-

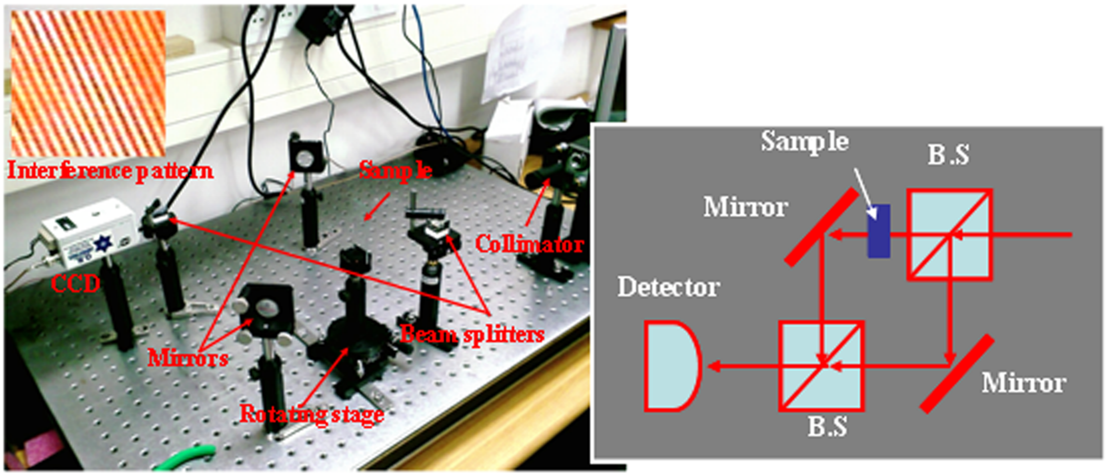

Fig. 6. (Color online) Experimental setup for the profile extraction concept based upon multiple angle projection.

pears in Fig. 7, where each pixel was $0.8\,\mu$m. Therefore the dimensions of the rectangle were about 0.7 mm by 2.4 mm. The profile height was approximately $10\,\mu$m (see Fig. 7 for a mesh chart).

Next we tried to verify the experimental data of Fig. 7 by applying our tomography-based approach. We used projection at two angles separated by 1 degree. The obtained results are seen in Fig. 8. In Fig. 8(a) one may see the two phase images obtained for the two projection angles. The phase images were obtained using digital holography. The algorithm was as follows: we performed a Fourier transform over the recorded fringe pattern, and then we took out the information around the first diffraction order. We placed it around the center of the axes and performed an inverse Fourier transform. The obtained result was back free space propagated, using the Fresnel transform by the free space distance existing between the specimen and the recording array. The phase of the obtained distribution after the back free space propagation was extracted. In Fig. 8(b) we computed the profile of the sample. Each pixel in the figure is a pixel of the camera that is $6.7\,\mu$m by $6.7\,\mu$m. The thickness appearing in the figure is in meters.

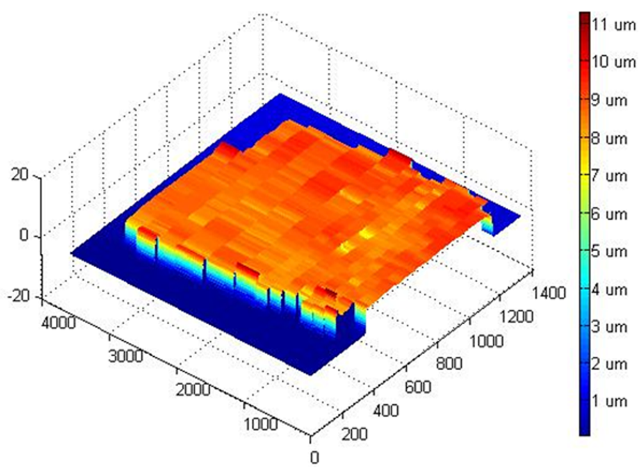

Fig. 7. (Color online) Experimental reconstruction using an Alpha-Step profile meter. Each pixel is $0.8\,\mu$m.

One may see that the results obtained using digital holography with multiple projections correspond well to the experimental measurements of Fig. 7 both in the transversal dimensions of the phase segment (about 0.7 mm by 2.4 mm) and by its thickness (about $10\,\mu$m). Therefore, the proposed approach may be implemented in microscopy in extraction of profiles of transmissive phase objects (objects as biological cells).

4. Conclusions

In this paper we have demonstrated two approaches for extraction of the profiles and the 3D information of objects. In the first case we used an approach that is based upon the coherence property of the light source that affected the local contrast of the obtained interference fringes. From a single image we were capable of estimating the 3D information of a reflective object, and no scanning in time was required. The main advantage of this approach is that it fits well for real time object inspection, its accuracy does not depend on triangulation angle, and its axial precision can be tuned just by varying the spectral bandwidth of the light source and by changing its coherence length. In the second approach we have demonstrated a technique that has some similarity to tomography and that uses digital holography in order to extract the phase of transmissive objects from the plurality of slightly varied angles. Proper computation allows true estimation of the profile while solving the problem of the phase ambiguity due to phase wrapping every 2π. This approach allows imaging of phase-only transmissive objects, and in cases when the profile of the objects is known it allows estimating its refraction index.

This work was supported by FEDER funds and the Spanish Ministerio de Educacion y Ciencia under the Project FIS2007-60626.

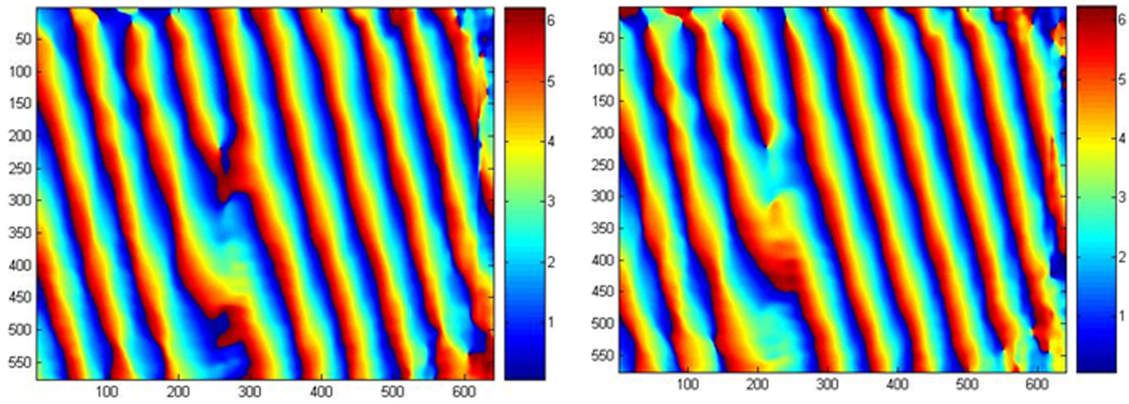

(a)

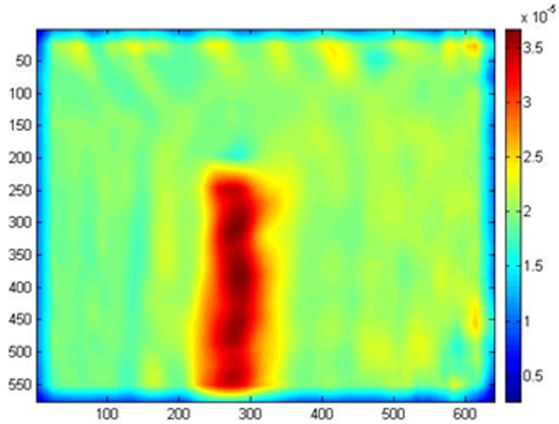

(b)

Fig. 8. (Color online) Experimental reconstruction. (a) Phase reconstruction for two projection angles that were separated by 1 degree. (b) Profile reconstruction. Each pixel is the pixel of the camera that was 6.7 μm. The alleviation thickness is in meters.

References

1. Y. G. Leclerc and A. F. Bobick, "The direct computation of height from shading," in IEEE Conference on Computer Vision & Pattern Recognition (IEEE, 1991), pp. 552–558.
2. R. Zhang and M. Shah, "Shape from intensity gradient," IEEE Trans. Syst. Man Cybern., Part A Syst. Humans **29**, 318 (1999).
3. "Height recovery from intensity gradients," in IEEE Conference on Computer Vision & Pattern Recognition (IEEE, 1994), pp. 508–513 .
4. B. K. P. Horn, "Height and gradient from shading," Int. J. Comput. Vis. **5**, 37–76 (1990).
5. A. M. Bruckstein, "On shape from shading," Comput. Vis. Graph. Image Process. **44**, 139–154 (1988).
6. M. Asada, H. Ichikawa, and S. Tjuji, "Determining of surface properties by projecting a stripe pattern," in Proceedings of the International Pattern Recognition Conference (IEEE, 1986), pp.1162–1164.
7. M. Asada, H. Ichikawa, and S. Tsuji, "Determining surface orientation by projecting a stripe pattern," IEEE Trans. Pattern Anal. Mach. Intell. **10**, 749–754 (1988).
8. S. Winkelbach and F. M. Wahl, "Shape from single stripe pattern illumination," in *(DAGM 2002) Pattern Recognition*, Vol. 2449 of Lecture Notes in Computer Science, L. Van Gool, ed. (Springer, 2002), pp. 240–247.
9. T. P. Koninckx and L. Van Gool, "Efficient, active 3D acquisition, based on a pattern-specific snake," in *(DAGM 2002) Pattern Recognition*, Vol. 2449 of Lecture Notes in Computer Science, L. Van Gool, ed. (Springer, 2002), pp. 557–565.
10. R. Kimmel, N. Kiryati, and A. M. Bruckstein, "Analyzing and synthesizing images by evolving curves with the Osher-Sethian method," Int. J. Comput. Vis. **24**, 37–56 (1997).
11. G. Zigelman, R. Kimmel, and N. Kiryati, "Texure mapping using surface flattening via multi-dimensional scaling," IEEE Trans. Vis. Comput. Graph. **8**, 198–207 (2002).
12. L. Zhang, B. Curless, and S. M. Seitz, "Rapid shape acquisition using color structured light and multi pass dynamic programming," presented at the 1st International Symposium on 3D Data Processing Visualization and Transmission (3DPVT), Padova, Italy, July, 2002.
13. P. Besl, "Active optical range imaging sensors," Mach. Vision Applications **1**, 127–152 (1988).
14. E. Horn and N. Kiryati, "Toward optimal structured light patterns," presented at the International Conference on Recent Advances in 3-D Digital Imaging and Modeling, Ottawa, Canada, May 1997.
15. T. Sawatari,, "Real-time noncontacting distance measurement using optical triangulation," Appl. Opt. **15**, 2821–2827 (1976).

16. G. Hausler and D. Ritter, "Parallel three-dimensional sensing by color-coded triangulation," Appl. Opt. **32**, 7164–7170 (1993).
17. R. G. Dorsch, G. Hausler, and J. M. Herrmann, "Laser triangulation: fundamental uncertainty in distance measurement," Appl. Opt. **33**, 1306–1312 (1994).
18. D. Sazbon, Z. Zalevsky, and E. Rivlin, "Qualitative real-time range extraction for preplanned scene partitioning using laser beam coding," Pattern Recogn. Lett. **26**, 1772–1781 (2005).
19. D. Gabor, "Microscopy by reconstructed wave fronts," Proc. R. Soc. London, Ser. A **197**, 454–487 (1949).
20. E. N. Leith, "Overview of the development of holography" J. Imaging Sci. Technol. **41**, 201–204 (1997).
21. E. N. Leith and J. Upatnieks, "Wavefront reconstruction and communication theory," J. Opt. Soc. Am. **52**, 1123–1130 (1962).
22. Y. N. Denisyuk, "On the reproduction of the optical properties of an object by the wave fields of its scattered radiation," Opt. Spectrosc. **15**, 279–284 (1964).
23. R. V. Pole, "3-D imaging and holograms of objects illuminated in white light," Appl. Phys. Lett. **10**, 20–22 (1967).
24. A. Stern and B. Javidi, "Improved-resolution digital holography using the generalized sampling theorem for locally band-limited fields," J. Opt. Soc. Am. A **23**, 1227–1235 (2006).
25. U. Schnars and W. P. O. Juptner, "Digital recording and numerical reconstruction of holograms," Meas. Sci. Technol. **13**, R85–R101 (2002).
26. T. Colomb, F. Montfort, J. Kühn, N. Aspert, E. Cuche, A. Marian, F. Charrière, S. Bourquin, P. Marquet, and C. Depeursinge, "Numerical parametric lens for shifting, magnification, and complete aberration compensation in digital holographic microscopy," J. Opt. Soc. Am. A **23**, 3177–3190 (2006).
27. C. Mann, L. Yu, C. -M. Lo, and M. Kim, "High-resolution quantitative phase-contrast microscopy by digital holography," Opt. Express **13**, 8693–8698 (2005).
28. E. Cuche, F. Bevilacqua, and C. Depeursinge, "Digital holography for quantitative phase-contrast imaging," Opt. Lett. **24**, 291–293 (1999).
29. P. Ferraro, S. De Nicola, A. Finizio, G. Coppola, S. Grilli, C. Magro, and G. Pierattini, "Compensation of the inherent wave front curvature in digital holographic coherent microscopy for quantitative phase-contrast imaging," Appl. Opt. **42**, 1938–1946 (2003).
30. I. Yamaguchi and T. Zhang, "Phase shifting digital holography," Opt. Lett. **22**, 1268–1270 (1997).
31. J. H. Bruning, D. R. Herriot, J. E. Gallagher, D. P. Rosenfeld, A. D. White, and D. J. Brangaccio, "Digital wavefront measuring interferometer for testing optical surfaces and lenses," Appl. Opt. **13**, 2693–2703 (1974).
32. C. Iemmi, A. Moreno, and J. Campos, "Digital holography with a point diffraction interferometer," Opt. Express **13**, 1885–1891 (2005).
33. W. Xu, M. H. Jericho, I. A. Meinertzhagen, and H. J. Kreuzer, "Digital in-line holography of microspheres," Appl. Opt. **41**, 5367–5375 (2002).
34. J. Garcia-Sucerquia, W. Xu, S. K. Jericho, P. Klages, M. H. Jericho, and H. J. Kreuzer, "Digital in-line holographic microscopy," Appl. Opt. **45**, 836–850 (2006).
35. E. Cuche, P. Marquet, and C. Depeursinge, "Simultaneous amplitude-contrast and quantitative phase-contrast microscopy by numerical reconstruction of Fresnel off-axis holograms," Appl. Opt. **38**, 6994–7001 (1999).
36. P. Marquet, B. Rappaz, P. J. Magistretti, E. Cuche, Y. Emery, T. Colomb, and C. Depeursinge, "Digital holographic microscopy: a noninvasive contrast imaging technique allowing quantitative visualization of living cells with subwavelength axial accuracy," Opt. Lett. **30**, 468–470 (2005).
37. B. Kemper and G. von Bally, "Digital holographic microscopy for live cell applications and technical inspection," Appl. Opt. **47**, A52–A61 (2008).
38. B. Rappaz, P. Marquet, E. Cuche, Y. Emery, C. Depeursinge, and P. Magistretti, "Measurement of the integral refractive index and dynamic cell morphometry of living cells with digital holographic microscopy," Opt. Express **13**, 9361–9373 (2005).
39. V. Mico, J. García, C. Ferreira, D. Sylman, and Z. Zalevsky, "Spatial information transmission using axial temporal coherence coding," Opt. Lett. **32**, 736–738 (2007).
40. J. Rosen and A. Yariv, "General theorem of spatial coherence: application to three-dimensional imaging," J. Opt. Soc. Am. A **13**, 2091–2095 (1996).
41. D. Huang, E. A. Swanson, C. P. Lin, J. S. Schuman, W. G. Stinson, W. Chang, M. R. Hee, T. Flotte, K. Gregory, C. A. Puliafito, and J. G. Fujimoto, "Optical coherence tomography," Science **254**, 1178 (1991).
42. J. M. Schmitt, "Optical coherence tomography (OCT): a review," IEEE J. Sel. Top. Quantum Electron. **5**, 1205 (1999).
43. P. Massatsch, F. Charrière, E. Cuche, P. Marquet, and C. D. Depeursinge, "Time-domain optical coherence tomography with digital holographic microscopy," Appl. Opt. **44**, 1806–1812 (2005).
44. G. Pedrini and S. Schedin, "Short coherence digital holography for 3D microscopy," Optik (Jena) **112**, 427–432 (2001).
45. F. Charrière, A. Marian, F. Montfort, J. Kuehn, T. Colomb, E. Cuche, P. Marquet, and C. Depeursinge, "Cell refractive index tomography by digital holographic microscopy," Opt. Lett. **31**, 178–180 (2006).
46. F. Charrière, N. Pavillon, T. Colomb, C. Depeursinge, T. J. Heger, E. A. D. Mitchell, P. Marquet, and B. Rappaz, "Living specimen tomography by digital holographic microscopy: morphometry of testate amoeba," Opt. Express **14**, 7005–7013 (2006).
47. W. Choi, C. Fang-Yen, K. Badizadegan, R. R. Dasari, and M. S. Feld, "Extended depth of focus in tomographic phase microscopy using a propagation algorithm," Opt. Lett. **33**, 171–173 (2008).
48. T. Dresel, G. Hausler, and H. Venzke, "Three-dimensional sensing of rough surfaces by coherence radar," Appl. Opt. **31**, 919–925 (1992).
49. H. Stark and H. Peng, "Shape estimation in computer tomography from minimal data," J. Opt. Soc. Am. A **5**, 331–337 (1988).
50. T. Yasokawa, I. Ishimaru, M. Kondo, S. Kuriyama, T. Masaki, K. Takegawa, and N. Tanaka, "A method for measuring the three-dimensional refractive index distortion of single cell using proximal two-beam optical tweezers and a phase shifting Mach-Zehnder interferometer," Opt. Rev. **14**, 161–164 (2007).
51. B. Kemper, S. Kosmeier, P. Langehanenberg, G. Von Bally, I. Bredebusch, W. Domschke, and J. Schnekenburger, "Integral refractive index determoination of living suspension cells by multifocus digital holographic phase contrast microscopy," J Biomed. Opt. **12**, 054009 (2007).
52. N. Lue, G. Popescu, T. Ikeda, R. R. Dasari, K. Badizadegan, and M. S. Feld, "Live cell refractometry using microfluidic devices," Opt. Lett. **31**, 2759–2761 (2006).
53. M. M. Hossain, D. S. Mehta, and C. Shakher, "Refractive index determination: an application of lensless Fourier digital holography," Opt. Eng. **45**, 106203–106207 (2006).